THE JOURNAL OF PHYSICAL CHEMISTRY C

Article

pubs.acs.org/JPCC

Structural and Energetic Trends of Ethylene Hydrogenation over Transition Metal Surfaces

Christopher J. Heard,* Samira Siahrostami, and Henrik Grönbeck

Department of Applied Physics and Competence Centre for Catalysis, Chalmers University of Technology, Göteborg 412 58, Sweden

ABSTRACT: Density functional theory calculations are used to investigate the catalytic hydrogenation of ethylene to ethane over a wide range of transition metal (TM) surfaces. Assuming the Horuiti−Polanyi mechanism, the enthalpies of adsorption, surface diffusion, and hydrogenation barriers are examined over close-packed surfaces of Co, Ni, Cu, Ru, Rh, Pd, Ag, Os, Ir, Pt, and Au. Special attention is given to the effects of ethylene and hydrogen coverage on the reaction pathway and activation energies. The previously suggested importance of the balance between di-σ and π adsorption modes is reinvestigated, and most metals are found to exhibit a preference for the π state. Hydrogen coverage is found to control the reactant stability and promote a surface distortion which facilitates the hydrogen addition reaction. For all TMs, the calculated activation energies are low and span a narrow range.

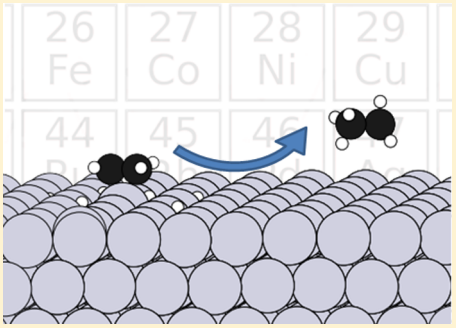

Downloaded via UNIV OF CALGARY on January 4, 2021 at 15:04:30 (UTC).
See https://pubs.acs.org/sharingguidelines for options on how to legitimately share published articles.

INTRODUCTION

The catalytic hydrogenation of alkenes is a major process in industrial chemistry, utilized in such diverse areas as food preparation, cosmetics, and fuel processing.[1] Within the automotive industry, hydrogenation is crucial to enhance the stability of biofuel feedstocks. Biofuels, derived from organic sources, contain a mixture of saturated and unsaturated esters of varying carbon chain lengths that are unstable with respect to oxidation under ambient atmospheric conditions. Understanding and controlling the processes by which this stability may be chemically enhanced is of major present concern.[2−4] To this end, the activity of heterogeneous catalysts toward the reduction of the carbonyl functional group is a primary focus.[5−8] Furthermore, selectivity of the catalyst toward the carbonyl group rather than the alkene groups is key to the design of appropriate catalysts. To control the selectivity it is necessary to understand the governing factors for both alkene and carbonyl hydrogenation.

Hydrogenation of alkenes over metal surfaces has been studied in the past with ethylene as a model reactant.[9−13] The primary mechanism for hydrogenation of simple alkenes over metal surfaces has been established as the Horuiti−Polanyi (HP) reaction.[14−17] In this scheme, the alkene is adsorbed on the surface, and two sequential hydrogen addition steps take place from a reservoir of adsorbed hydrogen atoms. The resulting alkane desorbs spontaneously and the supply of hydrogen is restocked by the dissociative chemisorption of gaseous H_2.

Although the overall reaction mechanism on different metal surfaces is known to follow the HP scheme, it has been difficult to establish unambiguous trends across the periodic table.[10,18,19] First-principles calculations have the ability to isolate various factors that may influence the mechanism through which the reaction proceeds. In this work, we undertake a density functional theory analysis of the HP hydrogenation pathway of ethylene (C_2H_4) to ethane (C_2H_6) over 11 late transition metals (TMs). By comparing a wide range of metals, we elucidate structural and energetic trends across the periodic table. The chemisorption properties of ethylene, ethyl, and hydrogen are examined, along with the effect of reactant coverages on stability and binding mode preference. Transition states are calculated along the reaction pathway and used to generate the full reaction profiles. Finally, the correlation between energetic and electronic parameters is discussed.

BACKGROUND

Early experiments by Beeck and co-workers[9,18,20,21] aimed to isolate the primary factors which control the hydrogenation reaction. The activity was correlated with the lattice parameter of the various TMs and found to be structure-sensitive for nickel.[22] In addition, the arrangement of reactive species on the surface was proposed to be important for the reaction.[22]

The question of which species are present on the TM surface under particular conditions has generated much interest, with many experimental and theoretical studies performed to identify the range of carbonaceous intermediates and their possible role on the hydrogenation reaction.[23−26] One issue in catalytic hydrogenation of alkenes is that catalysts which are active for hydrogenation are also active for dehydrogenation. This fact leads to the possibility of a rich surface chemistry with competing reaction mechanisms. One example is the so-called self-hydrogenation, where hydrogen atoms released through alkene dehydrogenation react with another alkene moiety. On Pt(111), dissociative chemisorption of ethylene to ethylidyne (CH_2CH) has been observed with low-energy electron

Received: October 5, 2015
Published: December 10, 2015

 © 2015 American Chemical Society

DOI: 10.1021/acs.jpcc.5b09735
J. Phys. Chem. C 2016, 120, 995−1003

diffraction (LEED), reflection−absorption infrared spectroscopy (RAIRS), temperature-programmed desorption (TPD), and X-ray absorption spectroscopic experiments,[10,27−29] suggesting a saturation coverage of 25%. A layer of ethylidyne is known to form over many late TMs at room temperature, including Ru(001),[30] Ir(111),[31] Pd(111),[32−35] Rh(111),[36,37] and Ni(111).[38] Helium scattering measurements suggested that ethylene binds upon the ethylidyne layer over Pt(111).[39] Such an adsorption mode raises the possibility of an additional mechanism for hydrogenation, namely, that ethylidyne is hydrogenated to ethylidene (CH_3CH), which further hydrogenates the adsorbed ethylene to ethane. Theoretical analysis by Anderson and Choe showed, however, that this pathway is thermodynamically unfeasible[40] and ethylidyne was experimentally later identified as a spectator species.[41] Ethylidyne has been calculated[40] and measured[42] to be mobile on Pt(111) which allows for ethylene to be hydrogenated according to the conventional HP mechanism.

Ethylene can adsorb on metal (M) surfaces in two modes, namely, di-σ and π. The di-σ mode involves a reduction of the ethylene C−C bond order, from 2 to 1, and the formation of two C−M σ bonds. Thus, this mode involves the rehybridization of ethylene from sp^2 to sp^3 and occupies two metal sites. In the π mode, ethylene adsorbs to a single metal atom, and the molecule is not significantly rehybridized.[43,44] The competition between the binding modes and their role in the hydrogenation reaction has been discussed extensively,[45−50] and both modes have been detected and analyzed experimentally (see, e.g., ref 51). For example, the π mode has been observed on Pd(111) at low temperatures by use of angle-resolved ultraviolet photoelectron spectroscopy (ARUPS).[33] The molecules were measured to adsorb with a high sticking coefficient up to a maximum coverage of 33%. Stacchiola et al. later showed a particle size dependence of the π preference over Pd nanoparticles.[52] Larger particles were suggested to exhibit a greater propensity toward back-bonding charge transfer to ethylene, which in turn promotes rehybridization, yielding an increase in the di-σ/π ratio. Computational studies have also shown a competition between di-σ and π modes over Pd(111). Due to effects of lateral repulsion between the adsorbates, it has been suggested that the mode preference is coverage-dependent.[43,46] A similar di-σ and π coexistence has been reported for several metal surfaces where Pt(111) is one example.[28]

In general, nondissociative ethylene chemisorption may take either mode, although the π state is considered the most active mode for HP hydrogenation.[41,46,47] The preference for nondissociative adsorption of hydrocarbons onto metal surfaces was recognized by Silvestre and Hoffmann as a compromise between the strength of metal−adsorbate binding and the total strength of metal and adsorbate intrafragment binding.[53] The authors noted that multiple-site metal−adsorbate binding weakens the surface bonds most significantly and can promote dissociation of the molecule. Nondissociative chemisorption, and similarly the absence of surface distortion, occurs over metals to which the adsorbate occupies only one metal site.

Hydrogenation activity trends of metal surfaces have been discussed in terms of electronic structure. One early contribution is the resonance d-band model of Pauling[54,55] which predicted that metals with a high "d-contribution" in their metal−metal bonding made better catalysts owing to their advantageous adsorption properties. Later theoretical analysis of the adsorption and hydrogen insertion processes for ethylene on 4d metals went further, and it was found that ethylene adsorbed more strongly to metals with high d-occupation due to a combination of spin pairing and exchange energy effects which balance the costs of covalent and donor type bonds.[19,44] The lowest H insertion barrier was calculated for Rh and was found to be related to a small metal promotion energy which minimized repulsion between metal s electrons and the ethylene frontier orbitals.

In addition to the importance of ethylene adsorption, the role of hydrogen coverage on the metal surface during the hydrogenation reaction has been stressed.[13,56,57] By use of TPD, it has been observed that codosing H_2 with ethylene reduces the apparent activation energy and increases ethane yield over Pt(111).[13,56] Shaikhutdinov et al. performed a TPD analysis of ethylene adsorption on Pd nanoparticles,[57] observing that dosing hydrogen caused a change in the distribution of di-σ to π modes for ethylene. It was suggested that the blocking of Pd hollow sites by hydrogen promotes the π state, which leads to an increased activity. Similar results were obtained with RAIRS by Stacchiola et al.[52] on Pd(111), who reported a shift from di-σ to π upon hydrogen preloading and a small (0.13 eV) apparent activation energy for the hydrogenation reaction. Furthermore, the reaction was found to be suppressed upon codosing of ethylene and hydrogen which indicates that ethylene may block hydrogen adsorption. Similar conclusions have been made for ethylene hydrogenation over Pt[13] and Ni.[58]

The extent to which adsorption energies control ethylene hydrogenation has been questioned since the earliest studies by Beeck,[9] and later work aimed to identify the relevant kinetic mechanisms. For example, Bos and Westerterp considered the selectivity of ethylene hydrogenation in competition with that of acetylene over Pd catalysts.[12] It was shown that adsorption energies do not account for the ethylene hydrogenation activity in the presence of ethyne and that a kinetic model with multiple adsorption sites is required to explain experimental results. Dumesic and co-workers developed a three-site kinetic model to describe ethylene hydrogenation over Pt(111)[59,60] which included competitive and noncompetitive adsorption sites. With this model it was possible to accurately reproduce turnover frequencies. However, the model is not fully consistent with the present atomistic understanding as it, for example, assumes hydrogenation from the di-σ mode.[60]

From the considerable amount of mechanistic work on ethylene hydrogenation, it is clear that the various ways in which ethylene and hydrogen bind and cover a surface are important in describing the full range of possibilities available to the reaction. Furthermore, the effects of reaction conditions, such as the concentrations of reactants and how the catalyst is exposed to them, will likely influence the overall reaction mechanism.

■ COMPUTATIONAL DETAILS

Calculations are performed within density functional theory (DFT) as implemented in the Vienna ab initio package (VASP 5.2) using the Perdew, Burke, Ernerhof (PBE) functional.[61−65] The Kohn−Sham orbitals are expanded in a plane wave basis, truncated at an energy of 420 eV. Standard projected augmented wave potentials are utilized[66,67] to describe the interaction between the valence electrons and the core. Hydrogen and carbon atoms are treated with one and four electrons in the valence, respectively. For the group 8, 9, 10, and 11 metals, 8, 9, 10, and 11 electrons are treated explicitly. Integration over the Brillouin zone is approximated by finite

DOI: 10.1021/acs.jpcc.5b09735
J. Phys. Chem. C 2016, 120, 995−1003

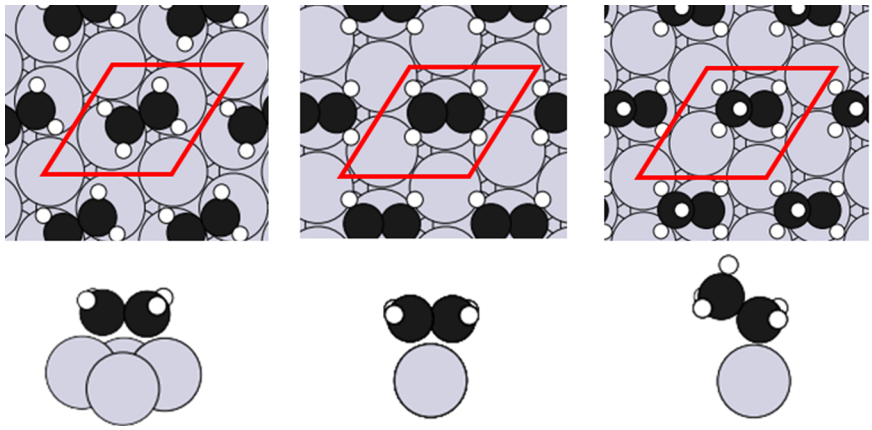

Figure 1. Structures of the di-σ ethylene (left), π ethylene (mid), and ethyl (right) binding modes over Pt(111) at a coverage of 33%. The top row corresponds to a top-down projection, while the bottom row is a side-view of the local geometry. The surface cell is indicated by dark lines.

sampling using the Monkhorst–Pack scheme,[68] and Methfessel and Paxton[69] smearing of the Fermi discontinuity is applied to first order, with a smearing width of 50 meV. Spin-unrestricted calculations are performed for metals with a nonzero bulk magnetic moment (Co and Ni), while all other calculations are restricted to a diamagnetic treatment. For local geometry optimization, the structures are considered to be converged when the energy differences are less than 1×10^{-3} eV and total forces are less than 1×10^{-2} eV/Å.

The metal surfaces were modeled with four-layer slabs separated by 20 Å of vacuum. Adsorption is considered in three types of surface cells, namely, $(\sqrt{3} \times \sqrt{3})R30°$, (2×2), and (3×3). With one ethylene adsorbed per cell, this corresponds to coverages of 33%, 25%, and 11%, respectively. It is notable that it was not possible to find stable adsorption structures for coverages higher than 33%, in agreement with TPD experiments over Pd(111).[33] We thereby justify considering 33% to be the high-coverage limit. The k-point grid is 7×7 for the smaller cell and 5×5 for the larger cells. The metals were treated in face-centered cubic (fcc) (111) (Ni, Cu, Rh, Pd, Ag, Ir, Pt, Au) or hexagonal close-packed (hcp) (0001) (Co, Ru, Os) bulk structures, respectively, which were cut from the theoretical bulk lattice optimized at the same level of theory.

The accuracy of the computational method for modeling the reactants was tested and the relaxed gas-phase C–C and C–H bond lengths in ethylene were found to be 1.33 and 1.09 Å, respectively, which is close to the experimental values of 1.33 and 1.08 Å. The corresponding theoretical (experimental) values for ethane are 1.53 (1.54) Å and 1.10 (1.11) Å.

Activation energies were calculated using the climbing-image nudged elastic band (CI-NEB) technique[70] as implemented in the transition state tools module for VASP. The number of images required to achieve convergence varied between five and eight for the various metals and intermediates, and all transition states located were confirmed with vibrational analysis.[71]

■ ADSORPTION OF REACTANTS

The binding of ethylene and ethyl species to the TM surfaces is calculated for both the di-σ and π modes. Figure 1 shows an example of the two bonding geometries for a coverage of 33% ethylene upon Pt(111). In agreement with previous theoretical studies, it is found that the C–C bond in the π mode is perfectly coplanar with the surface and is extended from the gas-phase value of 1.33 Å to 1.41 Å,[7,43,46] while the di-σ mode induces a larger C–C bond extension (to 1.49 Å). The trends in bond lengths across the investigated metals are reported in Table 1. For the metals with open d-shells, the C–M bond length is decreasing moving from left to right in the periodic table. Adsorption on the coinage metals results in long C–M distances which is a structural signature of physisorbed molecules. This is due to repulsion between the occupied valence s states on the metal and the sp^2 orbitals of ethylene.[72] Concerning the C–C bond, the di-σ mode always causes a greater extension with respect to the gas phase than the π mode. The difference between the C–C bond in the two modes is particularly large for the metals where ethylene is preferably adsorbed in the di-σ mode.

Table 1. C–C and C–M Bond Distances (Angstroms) over TMs at 33% Ethylene Coverage, with Overall Binding Mode Preference[a]

metal	C–C (π)	C–C (di-σ)	C–M (π)	C–M (di-σ)	preferred mode
Co	1.41	1.43	2.04	2.05	π
Ni	1.40	1.44	2.03	2.01	π
Cu	1.38	1.39	2.22	2.25	π
Ru	1.43	1.47	2.20	2.19	π
Rh	1.41	1.46	2.15	2.14	π
Pd	1.38	1.45	2.20	2.13	di-σ
Ag	1.34	1.34	3.46	3.53	
Os	1.43	1.50	2.24	2.19	π/di-σ
Ir	1.42	1.50	2.18	2.15	di-σ
Pt	1.41	1.49	2.17	2.11	di-σ
Au	1.33	1.33	3.55	3.74	

[a]The gas-phase C–C length is 1.33 Å.

Our results for ethylene adsorption on the metal surface are in good agreement with available theoretical and experimental data.[29,44,73] For example, by use of He II photoemission spectroscopy in combination with Hartree–Fock calculations, Demuth estimated the C–C bond lengths to be 1.39, 1.47, and 1.52 Å, for ethylene adsorbed upon Ni(111), Pd(111), and Pt(111), respectively.[73] The HCH bond angles suggested π, di-σ, and di-σ adsorption modes for the three metals, respectively. Both the bond lengths and the site preference are in agreement with our results. By extended X-ray absorption fine structure (EXAFS), the C–C bond length on Pt(111) was later determined to be 1.49 ± 0.04 Å.[29] For the 4d metals Ru, Rh, and Pd, the π mode may be compared with the theoretical

DOI: 10.1021/acs.jpcc.5b09735
J. Phys. Chem. C 2016, 120, 995–1003

results of Blomberg et al.,[44] who report C−C lengths of 1.44, 1.44, and 1.43 Å, respectively, for adsorption on metal atoms. Care should be taken in comparing the binding to a single metal atom with that over an extended surface, but it is clear that, for the π mode, the single atom gives a fair representation of the geometry.

The adsorption energies of ethylene (π and di-σ modes), ethyl, and hydrogen upon the surfaces at one-third coverage are

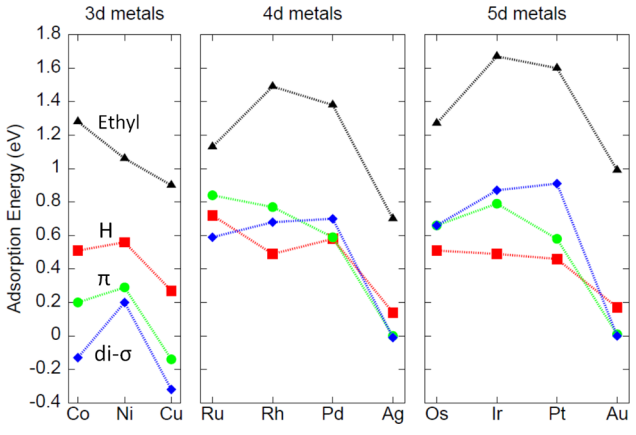

Figure 2. Adsorption energies of the di-σ ethylene (blue diamonds), π ethylene (green circles), H (red squares), and ethyl (black triangles) species for the investigated TMs, at a coverage of 33%.

depicted in Figure 2. The adsorption energy for an adsorbate X is calculated according to

$$E_{ads} = -(E_{tot} - E_{slab} - E_X) \quad (1)$$

where E_{tot} is the total energy of the chemisorbed adsorbate, E_{slab} is the total energy for the slab, and E_X is the total energy of the adsorbate in gas phase. Positive adsorption energies indicate exothermic adsorption. Focusing on ethylene, there is a general increase of the adsorption energy going from the 3d to the 5d metals. Within a period, there is a maximum in the adsorption energy for the di-σ mode at the d^9s^1 metals. The bonding to the coinage metals is weak, and a slightly endothermic adsorption energy is calculated for Cu(111). For this metal, a local minimum exists although the strain-induced energetic penalty in the metal and molecule is larger than the gain obtained by the metal−ethylene interaction. As a result, the C−Cu bond lengths (see Table 1) are clearly shorter than for the other coinage metals. This result is in agreement with previous calculations[74] as well as experimental near-edge X-ray absorption fine structure (NEXAFS) studies.[75]

There is an interesting trend in the competition between the π and di-σ modes across the periodic table. The di-σ mode becomes more stable moving from left to right and from 3d to 5d. As a consequence, it becomes the preferred mode for the late transition metals. Taking the examples of the d^9s^1 metals, the di-σ preference varies from −0.1 eV for Ni(111) to 0.1 and 0.3 eV for Pd and Pt, respectively. It is notable that an overall preference for the di-σ mode is observed only for Pd, Pt and Ir.

The bonding in the two modes is of a fundamentally different nature. The di-σ mode involves a rehybridization of the carbon centers from sp^2 to sp^3 and the subsequent overlap of sp^3 orbitals with metal d_{z^2} orbitals on adjacent atoms. In contrast, the π mode involves a flip of the p orbital phase on one carbon atom. This produce a net bonding interaction with a single metal p_{xz}/p_{yz} orbital. As a result, the π-adsorbed ethylene formally remains sp^2 hybridized and the C−C π bond is weakened, leading to an increased C−C bond length. For the di-σ bond, the rehybridization induces a more significant distortion and the C−C bond order is formally changed from 2 to 1. This view of the bonding is very similar to the one presented by Neurock and van Santen.[43]

Dissociative chemisorption, known to be the preferred mode of hydrogen adsorption over transition metals, is assumed across all metals in this study. CI-NEB calculations for H_2 dissociation were performed over Pd(111) and Pt(111) to determine whether the presence of ethylene blocks hydrogen diffusion and chemisorption. The calculations showed no barrier to adsorption for up to the maximum ethylene coverage of one-third. Atomic hydrogen adsorbs preferably in threefold hollow sites, with a slight (<50 meV) preference for fcc over hcp sites. The only exception is platinum, for which the atop site is competitive with the hollow sites.

The bond strength of hydrogen to the transition metals is largely invariant to the presence of more or less diffuse metal orbitals, and to the filling of the d-band, up to group 10. Therefore, the variation of hydrogen adsorption is unlikely to play a significant mechanistic role in ethylene hydrogenation. The only notable discrepancy is for adsorption on the coinage metals, Cu, Ag, and Au, which have a $d^{10}s^1$ electronic configuration. Coinage metals have low adsorption energies, with potentially high barriers to dissociative adsorption of hydrogen.[75−77] For gold surfaces, hydrogenation of acrolein has been recently proposed to follow a non-Horuiti−Polanyi mechanism where acrolein reacts with molecular hydrogen.[8]

There is an interesting trend when comparing the adsorption energies for hydrogen and ethylene between the rows of the period table. For 3d metals, hydrogen adsorption is clearly preferred over ethylene, while the opposite is true for 5d metals. The 4d metals display a subtle balance between hydrogen and ethylene preference, which suggests that operational control of the reaction conditions could be of importance. Preloading of either reactant has been shown experimentally to have an effect on the hydrogenation activity, as noted by Stacchiola et al.,[52] Shaikhutdinov et al.,[57] and Zaera.[56]

For the ethyl intermediate, the bonding arrangement involves a single C−metal bond to one atom in an atop fashion, see Figure 1, with higher adsorption energy than for ethylene, in part due to the instability of the gas-phase ethyl radical. Taking the example of Pt(111), the C−Pt bond length is calculated to be 2.09 Å, and the C−C bond length is 1.51 Å. This is in close agreement with previous calculations.[7,45,78] For the ethyl species, rehybridization to sp^3 carbon is complete, allowing a covalent interaction with metal d orbitals to produce an electronic shell closing stabilization. Co, Rh, and Ir represent local maxima in stability, as with an electronic d^9s^0 configuration, they are able to form a single covalent bond which induces a shell closing in both the carbon sp^3 and metal d shell, without the energetic cost of rehybridization.

Effects of Ethylene Coverage. It was noted in previous theoretical[43,46] and experimental[52,57] studies that the relative stability of the di-σ and π modes vary with adsorbate coverage on Pd and Pt surfaces; a high density of adsorbates drives a preference for the binding mode which occupies fewer metal sites. Thus, the π state should become stabilized at high ethylene coverages. We note that the di-σ mode is calculated to be the stable adsorption configuration for a coverage of 33%

DOI: 10.1021/acs.jpcc.5b09735
J. Phys. Chem. C 2016, 120, 995−1003

which is the experimentally observed saturation coverage for Pd(111)[33] (Figure 2).

In order to examine the dependence of the relative stabilities of the two adsorption modes, a lower loading of 25% over the pristine metal surface is considered. For Pt(111), an 11% ethylene coverage is additionally investigated. In general, the preferred adsorption mode is the same for the studied coverages. Furthermore, as shown in Figure 3, the relative

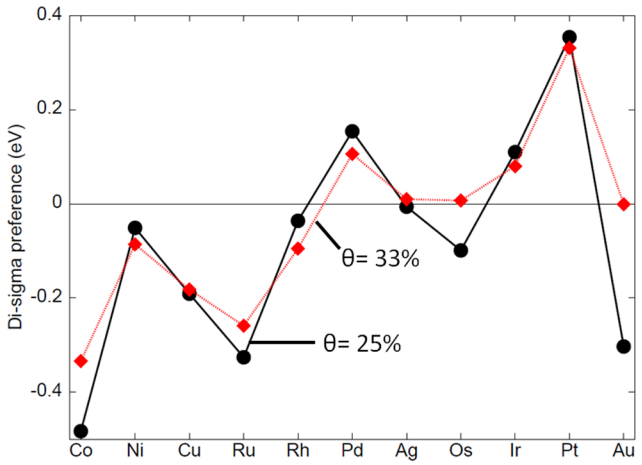

Figure 3. Ethylene adsorption preference over the studied metals at coverages of 33% (red diamonds) and 25% (black circles). Preference for the di-σ mode is denoted by positive values.

preference between the two modes displays a lack of coverage dependence. Most metals exhibit a change of less than 0.1 eV in total mode preference, with exceptions for Co and Au. For these metals, the effect may be ascribed primarily to the weak adsorption at 33% coverage. For Pt at 11%, the di-σ preference is determined to be 0.29 eV, which is similar to that for 25% (0.35 eV) or 33% (0.33 eV). This result agrees with that of Hirschl et al.[7] for 25% coverage, where a di-σ preference of 0.37 eV was reported. It is obvious that the ethylene coverage is not the sole driving force toward promotion of the π state, which is expected to be the intermediate species for the hydrogenation reaction. The trends across the periodic table are clear, with distinct peaks in the di-σ preference for the platinum group metals, and minima for the group 8 metals. Moreover, there is a trend toward a di-σ preference moving down in the periodic table. This trend may be understood by the localized nature of the d orbitals for the 3d metals. The energetic trends are in agreement with the structural analysis in Table 1.

Effects of Hydrogen Coverage. The second important coverage dependence is that of hydrogen, which was varied independently of ethylene coverage. Taking the coverage of 25% ethylene, we examine the effect of hydrogen loading on the total and relative stability of the two ethylene binding modes. The coverage of hydrogen is here defined to be 25% for one hydrogen per cell, and 100% when all possible threefold sites are occupied. In this manner, the effect of lateral surface repulsion between hydrogen and ethylene species may be elucidated. Subsurface hydrogen, which is known to be the relevant adsorption mode for several metals,[79] is not considered, in order to identify trends which are general for all metals. We note that the diffusion barriers for H over TM surfaces are small. Consequently, H may easily migrate to sites near to ethylene.[80]

Figure 4 depicts the variation in ethylene adsorption energy with respect to the H precovered surface, given by

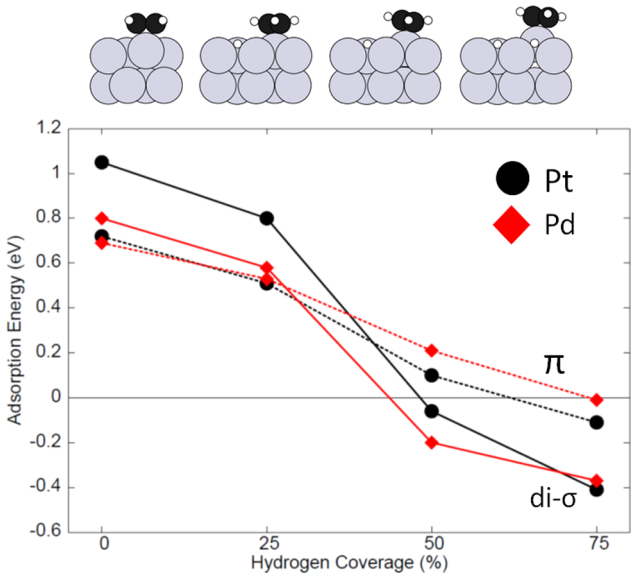

Figure 4. Effect of hydrogen loading for a fixed 25% ethylene coverage. Top: the resulting structural distortion on increasing H-loading from 0% to 75% on Pt(111). Bottom: ethylene adsorption energy as a function of H-loading in di-σ (solid) and π (dashed) modes, for Pd (red diamonds) and Pt (black circles).

$$E_{ads} = -(E_{tot} - E_{slab}^{nH} - E_{C_2H_4(g)}) \quad (2)$$

where E_{tot} is the total energy of the nH + C_2H_4 system and E_{slab}^{nH} is the total energy for the system with n chemisorbed H atoms. The effect of hydrogen loading for the adsorption energy of ethylene was calculated for Ni, Cu, Rh, Pd, Os, and Pt; however, for clarity only the results for Pd and Pt are shown in Figure 4.

For each metal, and for both binding modes, the total stability decreases dramatically with increasing H-loading and becomes unstable ($E_{ads} < 0$) at high coverage. The coverage at which adsorption becomes endothermic is metal-dependent. For Cu, E_{ads} is below zero for all H-coverages. For Os and Ni, ethylene adsorption becomes unfavorable between 25% and 50% H. Rh and Pt are stable to between 50% and 75%, while Pd only becomes unstable above 75% H coverage. In general, the di-σ mode is more dependent on H coverage than the π mode. This yields a coverage regime where the π mode is preferred. This effect is particularly striking for Pd and Pt, which exhibit a strong di-σ preference on the surface in the absence of hydrogen. Overall, rather than ethylene coverage alone, the preferred ethylene binding mode is shown to be sensitively dependent on metal and H-loading.

In addition to the energetic trend, it is noted that the coverage of hydrogen induces a local surface distortion, in which a metal atom is pulled out of the surface by the ethylene molecule. The effect is observed over all metals considered, and the surface rumpling is enhanced with H coverage. For 100% H loading, the local rumpling[81] ranges from 0.59 Å in Os, to 1.07 Å in Pt. Rh, Pd, and Ni have similar degrees of distortion, of 0.83, 0.87, and 0.91 Å, respectively. It is of note that the rumpled surface will geometrically promote the π mode. Thus, the di-σ configuration is disfavored structurally as well as energetically at high H loading.

DOI: 10.1021/acs.jpcc.5b09735
J. Phys. Chem. C 2016, 120, 995−1003

HYDROGENATION REACTION

The full reaction pathways for ethylene hydrogenation are investigated with an initial ethylene coverage of 33%. The reaction is studied according to the HP mechanism with the elementary steps $C_2H_4(ad) + H(ad) \rightarrow C_2H_5(ad)$ and $C_2H_5(ad) + H(ad) \rightarrow C_2H_6(g)$. The reaction pathways for Pt and Ru are shown in Figure 5. The two metals are chosen to

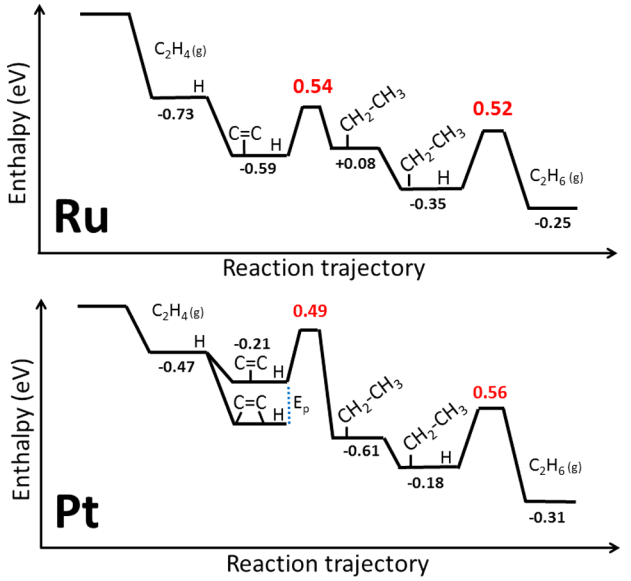

Figure 5. Reaction pathways for the hydrogenation of ethylene over Pt (top) and Ru (bottom) surfaces at 33% ethylene coverage. The energies differ for the two hydrogen adsorption steps because of the ethyl-hydrogen repulsion in the second step.

exemplify systems with π (Ru) and di-σ (Pt) preference. The pathways are calculated in a sequential manner, wherein the minimal hydrogen coverage required to allow the reaction is included at each stage. Therefore, the reaction profiles may be considered to represent the sparse hydrogen regime. The $C_2H_4(ad) + H(ad) \rightarrow C_2H_5(ad)$ step is calculated to proceed through the π state.[82] Thus, for the metals where ethylene preferably is adsorbed in the di-σ mode, a promotion energy (E_p) is defined as the difference in adsorption energy between the di-σ and π modes. The barrier for di-σ to π conversion was calculated according to a translation motion from bridge (di-σ) to atop (π) adsorbed ethylene and found to be small with respect to E_p. Thus, this step is not included in the reaction pathways.

The two reaction pathways are clearly different on Ru and Pt. The reactants are more strongly bonded to Ru than to Pt. Over Ru, the adsorption of hydrogen and ethylene is exothermic by 1.41 eV, making up the vast majority of the total reaction enthalpy. The first hydrogen addition step is actually slightly endothermic, while the addition of the second hydrogen is exothermic by only 0.25 eV. By contrast, the major energetic gain in the reaction over Pt is the first hydrogenation step, which is exothermic by 0.61 eV. Relative to the pristine surface and gas-phase reactants, the reaction pathway up to the formation of ethyl over Pt releases 1.27 eV, which makes up the majority of the total enthalpy of reaction, calculated to be 1.76 eV. The second hydrogen addition step is exothermic by 0.31 eV.

Comparing the barrier heights of Ru and Pt, we find that there is no clear difference, either between the first and second hydrogenation steps or the two metals. This result suggests that the first barrier may not be sufficient to represent the kinetics of the hydrogenation process. Over Pt, the accumulation of ethyl due to the higher second barrier is unlikely due to the high backward barriers from ethyl to ethylene and from ethane to ethyl. Our results predict that both Ru and Pt are active metals for ethylene hydrogenation, however, for slightly different reasons. In the case of Ru, the irreversible adsorption of the reactants will drive the reaction despite modest enthalpic gains along the reaction path. In contrast, for Pt every reaction step contributes to a similar extent to the enthalpy of the reaction.

Activation Energies. In general, a high activation barrier is indicative of a reaction step which is likely to limit the overall reaction rate. In order to investigate whether the hydrogenation barriers may control the reaction we have calculated the activation barriers for both hydrogenation steps for each TM, see Table 2. In all cases we find that the barriers are low. This is

Table 2. Transition State Barriers (eV) for the First and Second Hydrogen Addition Steps over the Investigated Metals[a]

metal	barrier 1	barrier 2
Co	0.41	0.51
Ni	0.25	0.22
Cu		
Ru	0.54	0.52
Rh	0.52	0.36
Pd	0.58	0.54
Ag		
Os	0.59	0.56
Ir	0.65	0.34
Pt	0.49	0.56
Au	0.57	0.50

[a]Converged reaction pathways are not found for the Cu and Ag surfaces.

in agreement with experimentally determined apparent activation energies for Co, Ni, Ru, Rh, Pd, Ir, and Pt.[10] Over this set, the average activation energy was reported to be 0.40 eV, with a standard deviation of 0.12 eV.[10] In comparison, our results show an average of 0.48 eV, and a standard deviation of 0.12 eV. The barriers for the 3d metals are slightly lower on average than for the 4d and 5d metals. In all cases, we observe that the calculated first and second hydrogenation barriers are similar. This suggests that both steps could be needed for a complete description of the reaction kinetics. We do not find any correlation between adsorption energies for the reactants and activation energies. This is in agreement with the conclusion of Siegbahn for hydrogen insertion to ethylene on single metal atoms.[19]

Analysis of the Transition States. The geometry of the first transition state is depicted in Figure 6 for Pd, while a schematic depiction of π ethylene and the first transition state for Ni, Ru, Rh, Pd, and Pt is included for comparison. The structure of the transition state has been discussed by several authors for the first addition step to π ethylene. Neurock et al. describe the geometry of the first transition state over Pd(111) at one-third π-ethylene coverage.[46] An early transition state was obtained,[46] in which the ethylene is coplanar with the surface, with a C−M bond of 2.16 Å, and a C−C bond of 1.41 Å. This

DOI: 10.1021/acs.jpcc.5b09735
J. Phys. Chem. C 2016, 120, 995−1003

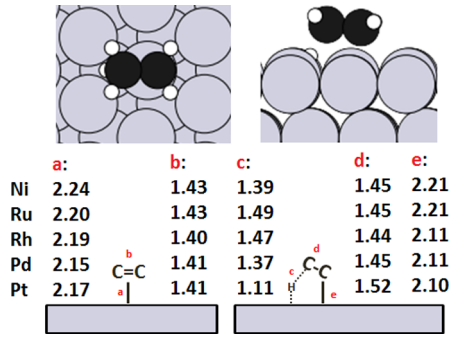

Figure 6. Top: transition state for the first hydrogen addition step from the π ethylene mode to ethyl over Pd(111). Bottom: a schematic of the π minimum and the first transition state over Ni, Ru, Rh, Pd, and Pt (top to bottom), with bond lengths in angstroms.

could be compared with the π ethylene-Pd(111) values of 2.20 and 1.38 Å, respectively.[46] Our results suggest a slightly later transition state, in which the C−M bond has contracted to 2.11 Å, and the C−C bond extended to 1.45 Å. The ethylene is therefore slightly further along the rehybridization path to form the sp^3 ethyl−metal system when the hydrogen addition takes place. Qualitatively, however, the process is similar, with a four-site transition state, between Pd, C, and H, and hydrogen in a twofold bridging site on the surface at the point of reaction. The barrier height obtained for this step is 0.58 eV (56.0 kJ/mol), which is higher than the 36 kJ/mol reported by Neurock et al. However, the transition state in ref 46 is not calculated from the stable π configuration, and thus the reported[46] activation energy is a lower bound.

The schematic in Figure 6 shows that for 3d, 4d, and 5d metals, the first transition state is generally fairly early along the reaction coordinate, with only a partial C−M bond contraction and C−C bond extension at the critical point. Furthermore, the pathway and the geometry of the transition states are similar across metals. The hydrogen migrates from the threefold hollow site to occupy a twofold bridge site at the transition state. An exception is Pt where H is located at an atop site in the transition state. We conclude that the hydrogen addition shows significant similarity across the late transition metals.

The second transition state is found to be later along the reaction coordinate, as displayed for Pd(111) in Figure 7. The hydrogen atom migrates from the threefold hollow site and

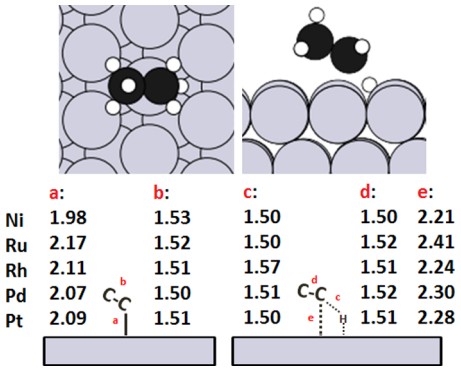

Figure 7. Top: transition state for the second hydrogen addition step from ethyl to ethane over Pd(111). Bottom: a schematic of the ethyl minimum and transition state over Ni, Ru, Rh, Pd, and Pt (top to bottom), with bond lengths in angstroms.

binds directly to the undercoordinated carbon atom in a concerted mechanism by which ethyl desorbs vertically from the surface, evolving into ethane as it desorbs. Over Rh and Pt, the second hydrogenation reaction involves a migration from a threefold to a bridge site before binding to ethyl. It can be observed from the bond lengths that the transition state is late, with C−M bonds extended by up to 0.27 Å before reaching the transition state. The C−C bonds show little variation in length, both across the metals and along the pathway. This is reasonable, as the ethyl C−C bond is effectively an ideal sp^3 single σ bond throughout the reaction.

DISCUSSION

Activation barriers are generally considered to be a metric for catalytic activity, in such a way that reduction of the rate-determining barrier will result in an increased reaction rate. In the past, this concept has also been applied to ethylene hydrogenation where emphasis has been put on the first hydrogenation step.[43] Furthermore, the relevance of reactant coverage on hydrogenation barriers has been suggested.[43,45] Specifically, a high ethylene coverage has been proposed to favor π-bonding from which the hydrogenation reaction proceeds with a low barrier. By studying ethylene hydrogenation over a range of TM surfaces, we are able to investigate the generality of these ideas across the periodic table.

We have calculated the hydrogenation barriers for $C_2H_4(ad) + H(ad) \rightarrow C_2H_5(ad)$ and $C_2H_5(ad) + H(ad) \rightarrow C_2H_6(g)$ over Co, Ni, Ru, Rh, Pd, Os, Ir, Pt, and Au. The two barriers are similar and in all cases low. Moreover, the complete reaction pathways do not support the focus on only the first hydrogenation step as representative of the overall reaction. The reaction barriers are found not to correlate with adsorption energies.

It is generally accepted that the first hydrogenation step proceeds via the π mode. Therefore, it is important to understand under which conditions this mode is preferred. This is, in particular, true for Pd, Ir, and Pt, which have a di-σ preference on the clean metal surfaces which is not significantly dependent on ethylene coverage. We find, however, a dependence of the preferred mode on the hydrogen coverage. A high hydrogen coverage promotes the π mode. Furthermore, there is a metal dependence on the maximum hydrogen coverage that allows simultaneous ethylene adsorption. This is an important observation, as it has a implications on the likely coverages available in the experiment and the energetics of the reaction.

Experimental studies have previously noted the effects of preloading hydrogen onto the surface.[52,57] TPD results have, for example, suggested that the ethylene desorption temperature is reduced when the surface is exposed to hydrogen prior to ethylene. This is in agreement with our results for all TMs. Another effect of hydrogen loading is that it appears to inhibit ethylene decomposition.[57] Our calculations suggest that hydrogen loading is indeed likely to block ethylene decomposition. By introducing a surface distortion which disfavors the di-σ mode, from which C−C bond scission is known to occur, hydrogen serves to remove this reaction channel and, thus, may play an important kinetic role in ethylene hydrogenation. Furthermore, it may additionally be suggested that the extent of this distortion has a dependence on metal identity, complicating prediction of the prevalence of the π mode in practice.

DOI: 10.1021/acs.jpcc.5b09735
J. Phys. Chem. C 2016, 120, 995−1003

CONCLUSIONS

The reaction profiles, consisting of adsorption, reactant migration, sequential hydrogenation and desorption steps, have been modeled according to the HP mechanism. Small variations across the periodic table are predicted for the pathway, barrier heights, and transition state geometries. The latter are found to be early for the first hydrogenation reaction and later for the second step. The ability to dissociatively adsorb hydrogen in tandem with chemisorption of ethylene is expected to be the key requirement for the reaction to proceed, with activation and adsorption energies, along with the preferred location of adsorbed hydrogen, only secondary features of the reaction. Structural distortions of the surface are observed to be a general feature in high adsorbate coverage regimes. This appears to induce a synergistic effect, both to promote the active binding state of reactants and to disfavor unwanted side reactions, such as ethylene decomposition.

Work is currently being undertaken to model the kinetic properties of ethylene hydrogenation, in order to further isolate and explore factors involved in transition metal activity.

AUTHOR INFORMATION

Corresponding Author

*E-mail: christopher.heard@chalmers.se.

Notes

The authors declare no competing financial interest.

ACKNOWLEDGMENTS

The calculations were performed at C3SE (Göteborg) and PDC (Stockholm) under an SNIC grant. The work was supported by the Chalmers Area of Advance Transport and the Swedish Research Council. The Competence Centre for Catalysis (KCK) is hosted by Chalmers University of Technology and is financially supported by the Swedish Energy Agency and the member companies: AB Volvo, ECAPS AB, Haldor Topsøe A/S, Scania CV AB, Volvo Car Corporation AB, and Wärtsilä Finland Oy. The authors acknowledge support from the Nordforsk programme: an interdisciplinary approach to atomistic design of new catalysts.

REFERENCES

(1) Zhang, Q.; Feldman, M.; Peterson, C. L. *Am. Soc. Agric. Eng.* **1988**, 88-1562.
(2) Monyem, A.; Canakci, M.; van Gerpen, J. H. *Appl. Eng. Agric.* **2000**, *16*, 373−378.
(3) Bouaid, A.; Martinez, M.; Aracil, J. *Fuel* **2007**, *86*, 2596−2602.
(4) Natarajan, E. *IJES* **2012**, *2*, 152−155.
(5) Gallezot, P.; Richard, D. *Catal. Rev.: Sci. Eng.* **1998**, *40*, 81−126.
(6) Delbecq, F.; Sautet, P. *J. Catal.* **2003**, *220*, 115−126.
(7) Hirschl, R.; Eichler, A.; Hafner, J. *J. Catal.* **2004**, *226*, 273−282.
(8) Yang, B.; Gong, X.-Q.; Wang, H.-F.; Cao, X.-M.; Rooney, J. J.; Hu, P. *J. Am. Chem. Soc.* **2013**, *135*, 15244−15250.
(9) Beeck, O. *Discuss. Faraday Soc.* **1950**, *8*, 118−128.
(10) Zaera, F.; Somorjai, G. A. *J. Am. Chem. Soc.* **1984**, *106*, 2288−2293.
(11) Fujikawa, K.; Kita, H.; Miyahara, K.; Sato, S. *J. Chem. Soc., Faraday Trans. 1* **1975**, *71*, 1573−1581.
(12) Bos, A. N. R.; Westerterp, K. R. *Chem. Eng. Process.* **1993**, *32*, 1−7.
(13) Godbey, D.; Zaera, F.; Yeates, R.; Somorjai, G. A. *Surf. Sci.* **1986**, *167*, 150−166.
(14) Horiuti, J.; Polanyi, M. *Nature* **1933**, *132*, 819−819.
(15) Horiuti, J.; Polanyi, M. *Nature* **1933**, *132*, 931−931.
(16) Horiuti, J.; Polanyi, M. *Nature* **1934**, *134*, 377−378.
(17) Horuiti, J.; Polanyi, M. *Trans. Faraday Soc.* **1934**, *30*, 1164−1172.
(18) Beeck, O. *Rev. Mod. Phys.* **1945**, *17*, 61−71.
(19) Siegbahn, P. E. M. *J. Am. Chem. Soc.* **1993**, *115*, 5803−5812.
(20) Beeck, O.; Ritchie, A. W. *Discuss. Faraday Soc.* **1950**, *8*, 159−166.
(21) Beeck, O.; Cole, W. A.; Wheeler, A. *Discuss. Faraday Soc.* **1950**, *8*, 314−321.
(22) Beeck, O.; Smith, A. E.; Wheeler, A. *Proc. R. Soc. London, Ser. A* **1940**, *177*, 62−90.
(23) Moskaleva, L. V.; Aleksandrov, H. A.; Basaran, D.; Zhao, Z.-J.; Rösch, N. *J. Phys. Chem. C* **2009**, *113*, 15373−15379.
(24) Zhao, Z.-J.; Moskaleva, L. V.; Aleksandrov, H. A.; Basaran, D.; Rösch, N. *J. Phys. Chem. C* **2010**, *114*, 12190−12201.
(25) Aleksandrov, H. A.; Moskaleva, L. V.; Zhao, Z.-J.; Basaran, D.; Chen, Z.-X.; Mei, D.; Rösch, N. *J. Catal.* **2012**, *285*, 187−195.
(26) Aleksandrov, H. A.; Kozlov, S. M.; Schauermann, S.; Vayssilov, G. N.; Neyman, K. M. *Angew. Chem., Int. Ed.* **2014**, *53*, 13371−13375.
(27) Somorjai, G. A.; Van Hove, M. A.; Bent, B. E. *J. Phys. Chem.* **1988**, *92*, 973−978.
(28) Steininger, H.; Ibach, H.; Lehwald, S. *Surf. Sci.* **1982**, *117*, 685−698.
(29) Stöhr, J.; Sette, F.; Johnson, A. L. *Phys. Rev. Lett.* **1984**, *53*, 1684−1687.
(30) Hills, M. M.; Parmeter, J. E.; Mullins, C. B.; Weinberg, W. H. *J. Am. Chem. Soc.* **1986**, *108*, 3554−3562.
(31) Marinova, T. S.; Kostov, K. L. *Surf. Sci.* **1987**, *181*, 573−585.
(32) Stacchiola, D.; Calaza, F.; Zheng, T.; Tysoe, W. T. *J. Mol. Catal. A: Chem.* **2005**, *228*, 35−45.
(33) Tysoe, W. T.; Nyberg, G. L.; Lambert, R. M. *J. Phys. Chem.* **1984**, *88*, 1960−1963.
(34) Kesmodel, L. L.; Gates, J. A. *Surf. Sci.* **1981**, *111*, L747−L754.
(35) Sock, M.; Eichler, A.; Surnev, S.; Andersen, J. N.; Klötzer, B.; Hayek, K.; Ramsey, M. G.; Netzer, F. P. *Surf. Sci.* **2003**, *545*, 122−136.
(36) Blackman, G. S.; Kao, C. T.; Bent, B. E.; Mate, C. E.; van Hove, M. A.; Somorjai, G. A. *Surf. Sci.* **1988**, *207*, 66−88.
(37) Köstner, R. J.; van Hove, M. A.; Somorjai, G. A. *Surf. Sci.* **1982**, *121*, 321−337.
(38) Zhu, X.-Y.; White, J. M. *Catal. Lett.* **1988**, *1*, 247−254.
(39) Weinberg, W. H.; Deans, H. A.; Merrill, R. P. *Surf. Sci.* **1974**, *41*, 312−336.
(40) Anderson, A. B.; Choe, S. J. *J. Phys. Chem.* **1989**, *93*, 6145−6149.
(41) Cremer, P. S.; Su, X.; Shen, Y. R.; Somorjai, G. A. *J. Am. Chem. Soc.* **1996**, *118*, 2942−2949.
(42) Land, T. A.; Michely, T.; Behm, R. J.; Hemminger, J. C.; Comsa, G. *Appl. Phys. A: Solids Surf.* **1991**, *53*, 414−417.
(43) Neurock, M.; van Santen, R. A. *J. Phys. Chem. B* **2000**, *104*, 11127−11145.
(44) Blomberg, M. R. A.; Siegbahn, P. E. M.; Svensson, M. *J. Phys. Chem.* **1992**, *96*, 9794−9800.
(45) Miura, T.; Kobayashi, H.; Domen, K. *J. Phys. Chem. B* **2000**, *104*, 6809−6814.
(46) Neurock, M.; Pallassana, V.; van Santen, R. A. *J. Am. Chem. Soc.* **2000**, *122*, 1150−1153.
(47) Cremer, P. S.; Somorjai, G. A. *J. Chem. Soc., Faraday Trans.* **1995**, *91*, 3671−3677.
(48) Ohtani, T.; Kubota, J.; Kondo, J. N.; Hirose, C.; Domen, K. *Surf. Sci.* **1998**, *415*, L983−L987.
(49) Kubota, J.; Ohtani, T.; Kondo, J. N.; Hirose, C.; Domen, K. *Appl. Surf. Sci.* **1997**, *121-122*, 548−551.
(50) Öfner, H.; Zaera, F. *J. Phys. Chem. B* **1997**, *101*, 396.
(51) Sheppard, N. *Annu. Rev. Phys. Chem.* **1988**, *39*, 589−644.
(52) Stacchiola, D.; Azad, S.; Burkholder, L.; Tysoe, W. T. *J. Phys. Chem. B* **2001**, *105*, 11233−11239.
(53) Silvestre, J.; Hoffmann, R. *Langmuir* **1985**, *1*, 621−647.
(54) Pauling, L. *The Nature of the Chemical Bond—An Introduction to Modern Structural Chemistry*, 3rd ed.; Cornell University Press: Ithaca, NY, 1960.
(55) Pauling, L. *J. Am. Chem. Soc.* **1931**, *53*, 1367−1400.

DOI: 10.1021/acs.jpcc.5b09735
J. Phys. Chem. C 2016, 120, 995−1003

(56) Zaera, F. *J. Phys. Chem.* **1990**, *94*, 5090−5095.
(57) Shaikhutdinov, S.; Heemeier, M.; Bäumer, M.; Lear, T.; Lennon, D.; Oldman, R. J.; Jackson, S. D.; Freund, H.-J. *J. Catal.* **2001**, *200*, 330−339.
(58) Laidler, K. J.; Townshend, R. E. *Trans. Faraday Soc.* **1961**, *57*, 1590.
(59) Cortright, R. D.; Goddard, S. A.; Rekoske, J. E.; Dumesic, J. A. *J. Catal.* **1991**, *127*, 342−353.
(60) Rekoske, J. E.; Cortright, R. D.; Goddard, S. A.; Sharma, S. B.; Dumesic, J. A. *J. Phys. Chem.* **1992**, *96*, 1880−1888.
(61) Kresse, G.; Hafner, J. *Phys. Rev. B: Condens. Matter Mater. Phys.* **1993**, *47*, 558.
(62) Kresse, G.; Hafner, J. *Phys. Rev. B: Condens. Matter Mater. Phys.* **1994**, *49*, 14251.
(63) Kresse, G.; Furthmüller, J. *Comput. Mater. Sci.* **1996**, *6*, 15.
(64) Kresse, G.; Furthmüller, J. *Phys. Rev. B: Condens. Matter Mater. Phys.* **1996**, *54*, 11169.
(65) Perdew, J. P.; Burke, K.; Ernzerhof, M. *Phys. Rev. Lett.* **1996**, *77*, 3865.
(66) Blochl, P. E. *Phys. Rev. B: Condens. Matter Mater. Phys.* **1994**, *50*, 17953.
(67) Kresse, G.; Joubert, D. *Phys. Rev. B: Condens. Matter Mater. Phys.* **1999**, *59*, 1758.
(68) Monkhorst, H. J.; Pack, J. D. *Phys. Rev. B* **1976**, *13*, 5188−5192.
(69) Methfessel, M.; Paxton, A. T. *Phys. Rev. B: Condens. Matter Mater. Phys.* **1989**, *40*, 3616−3621.
(70) Henkelman, G.; Uberuaga, B. P.; Jónsson, H. *J. Chem. Phys.* **2000**, *113*, 9901−9904.
(71) For CI-NEB calculations, Gaussian smearing was employed, exhibiting improved convergence, with a force convergence criterion of 50 meV/Å. Recalculation of the end point minima showed no significant change in geometry or energy for any system.
(72) Fournier, R. *J. Chem. Phys.* **1995**, *102*, 5396−5407.
(73) Demuth, J. R. *Surf. Sci.* **1979**, *84*, 315−328.
(74) Witko, M.; Hermann, K. *Appl. Catal., A* **1998**, *172*, 85−95.
(75) Fuhrmann, D.; Wacker, D.; Weiss, K.; Hermann, K.; Witko, M.; Wöll, Ch. *J. Chem. Phys.* **1998**, *108*, 2651−2658.
(76) Hammer, B.; Nørskov, J. *Surf. Sci.* **1995**, *343*, 211−220.
(77) Gross, A. *Surf. Sci. Rep.* **1998**, *32*, 291−340.
(78) Papoian, G.; Nørskov, J. K.; Hoffmann, R. *J. Am. Chem. Soc.* **2000**, *122*, 4129−4144.
(79) Yates, J. T.; Peden, C. H. F.; Houston, J. E.; Goodman, D. W. *Surf. Sci.* **1985**, *160*, 37−45.
(80) Hydrogen migration was calculated with CI-NEB for pathways between adjacent threefold hollow sites over pristine Pd(111) and Pt(111).
(81) Local rumpling is defined as the vertical deflection of the atom, relative to the position of it is nearest neighbours in the surface.
(82) Hydrogenation from the di-σ initial state was calculated over Pd(111). A spontaneous rearrangement to the π state was observed along the path.

DOI: 10.1021/acs.jpcc.5b09735
J. Phys. Chem. C 2016, 120, 995−1003